中國機械工程學刊第四十六卷第三期第 335~349 頁(民國一百一十四年)
Journal of the Chinese Society of Mechanical Engineers, Vol.46, No.3, pp 335~349 (2025)

Investigation of Electromechanical Coupling Modeling and Dynamic Characteristics of a Cutting System in Finishing Process Equipment

Li-Chen Shi*, Jie Yang** and He-Yuan Tian**

Keywords: finishing process, mechanical dynamics model, electromechanical coupling, dynamic characteristics.

ABSTRACT

In response to the challenging issue of titanium alloy wire processing, a finishing process equipment is used for surface turning and finishing processing. To improve the surface processing quality of the finishing equipment, an electromechanical coupling model is established, considering the interaction between the mechanical, electrical, and control systems. The accuracy of the mechanical dynamics model and the electromechanical coupling model is verified through experiments, and vibration characteristics are analyzed under the electromechanical coupling model. The study explores the system's dynamic characteristics under different motor speeds and feed rates, and investigates the impact of changes in mechanical parameters on system vibration. Experimental verification shows that the electromechanical coupling model more accurately reflects the real system characteristics. Vibration characteristics analysis reveals that with changes in motor speed and feed rate, the magnitude and trend of vibration in the cutting system also change. By comparing the error between the theoretical mean of displacement and the experimental value, the appropriate motor speed and feed rate are selected to improve the cutting efficiency and surface machining quality.

Paper Received November, 2024. Revised December, 2024. Accepted March, 2025. Author for Correspondence: Jie Yang

* *Professor, College of Mechanical and Electrical Engineering, Xi'an University of Architecture and Technology, Xi'an, 710055, China, email: beststlc@xauat.edu.cn*

** *Graduated Student, College of Mechanical and Electrical Engineering, Xi'an University of Architecture and Technology, Xi'an, 710055, China, email: susie0604@xauat.edu.cn*

** *Graduated Student, College of Mechanical and Electrical Engineering, Xi'an University of Architecture and Technology, Xi'an, 710055, China, email: tianheyuan@xauat.edu.cn*

INTRODUCTION

Due to their high strength-to-weight ratio and stability at high temperatures, TB9 titanium alloys are widely used in the aerospace, automotive, and other industries because they have high strength and are lightweight (Ren et al, 2020; Gao, 2020). However, its high hardness and low elastic modulus make it difficult to machine since it is prone to elastic deformation during processing, which significantly affects dimensional accuracy and surface quality (Li et al, 2018). To address these machining challenges, special machining methods are needed. Surface finishing, as a precision machining technology, seeks to increase dimensional accuracy and minimize surface roughness by removing a very thin layer of material. Surface turning is commonly used for finishing both domestically and internationally. This approach significantly enhances machining efficiency and reduces environmental pollution while ensuring surface machining quality. Finishing process equipment is very vulnerable to cutting chatter when turning small-diameter large-coil titanium alloy wires (Shi et al, 2022), and with its development to the direction of high power and integration, the mechanical vibration caused by the electromechanical coupling effect is more and more obvious. Therefore, understanding the chattering mechanism of the cutting system in finishing process equipment and the dynamic characteristics of its transmission system and electrical system is crucial for improving machining quality.

Numerous academics have investigated the behavior of vibration in the cutting process by establishing a cutting dynamics model to improve the stability of the system and the machining quality of the workpiece. OZLU et al. (2007a; b) concentrated on normal turning and established a dynamic model of the cutting system that takes the tool tip radius into account. The model's predictive results are found to be highly accurate compared to the experimental data. Y. Altintas et al. (2008) developed a time-periodic dynamic model of the milling process that summarizes

the frequency-domain and discrete-time-domain chatter patterns in milling operations. The model predicts the relationships between workpiece materials, machine tool structural dynamics, and cutting circumstances. Machine learning methods were also used to model dynamics in the field of high-precision machinery. References (Peng et al, 2024; Wang et al, 2024) used machine learning methods to model and predict the rotor behavior for the nonlinear behavior of the bearing system. References (Mishra et al, 2024) shows the impact of the cutting parameters on the carbon emissions of a three-axis milling machine and the carbon emissions data was predicted using various machine learning methods.

The transmission system of finishing equipment adopts synchronous belt transmission - a typical rotating mechanical power transmission method. Synchronous belts have higher transmission accuracy and load carrying capacity than flat belts, and have the advantages of low noise and no lubrication compared to chain drives (Qing et al, 2020). The establishment of an accurate dynamic model of synchronous belt transmission can effectively predict to the vibration response of the synchronous belt system transmission process, and its dynamic response has a greater impact on the overall system response. For synchronous belt transmission system, many scholars have carried out research. Reference (Zhu et al, 2021) studies on dynamic modeling, simulation and experiment of power transmission belt drives are comprehensively reviewed. Fu et al. (2023) propose a matrix model to calculate the tangential pressure of the meshing part between tooth and pulley, which solves the difficulty of calculating the tangential pressure of the belt. Wang et al. (2024) based on the viscoelastic characteristics of the synchronous belt, the influence of different pre-load and the plate load on the transverse vibration, load dynamic linear displacement error and motion characteristics of the synchronous belt was analyzed, which provides a theoretical reference for the application of similar devices in the optimization of PVC transmission accuracy and stability.

All of the above studies have investigated the vibration response problem by establishing the dynamics model of the mechanical system, while analyzing the dynamics of the mechanical system alone cannot fully take into account the motor and its control system, and cannot provide an accurate prediction of the system response. In recent years, scholars at home and abroad have conducted a lot of research in electromechanical coupling. Henao et al. (2003) based on the gearbox electromechanical system found that the torsional vibration of the gearbox has a more obvious effect on the electromagnetic torque and stator current, and the motor can be used as a torsional sensor to monitor the health status of the gears. Feki et al. (2012, 2013) proposed a new analytical formula of electromechanical coupling model based on the analysis of the current signals for the detection of gear faults. Kanaan et al. (2003) investigated the effect of different electromechanical parameters on the frequency response by analyzing the vibration frequency response of the system. Liu et al. (2014) studied the electromechanical coupling dynamic characteristics of a shearer cutting transmission system under unexpected load fluctuations. They obtained the patterns of influence of mechanical parameters on dynamic characteristics, which provided recommendations for mechanical parameter design. Chen et al. (2023) considered the nonlinear factors such as internal excitation of gears and electromagnetic excitation of motors in the electromechanical-rigid-flexible coupled dynamics model, and confirmed the accuracy of the model with the help of experiments. The aforementioned paper studies the electromechanical coupling characteristics of the motor-gear system, which differs from the motor-synchronous belt drive system in the finishing equipment discussed in this paper. Moreover, the load mechanism at the other end of the synchronous belt transmission system is the cutting system, and the fluctuation of the motor torque directly excites the transmission system, which in turn affects the vibration characteristics of the cutting system, and the cutting system also affects the electrical system current and other changes that occur to form a coupled vibration system, and its dynamic characteristics are also richer.

This paper takes the power cutting system of finishing process equipment as the research object, establishes the dynamic model of cutting system, the dynamic model of torsional vibration of synchronous belt transmission system and the model of permanent magnet synchronous motor respectively, and establishes the electromechanical coupling model of the power cutting system with the link of electromagnetic torque. The influence of mechanical parameters on the vibration characteristics of the power cutting system is studied, and the correctness of the electromechanical coupling model is verified through tests.

DYNAMIC MODELING OF CUTTING SYSTEMS FOR FINISHING PROCESS EQUIPMENT

The finishing process equipment is primarily composed of multiple components, including an electric machine, a synchronous belt drive mechanism, a hollow spindle, a front guide mechanism, a middle and rear guide mechanism, and a cutterhead cutting system. Fig. 1 illustrates all of these components. Subsystem modeling and analysis are required for correct characterization of the overall system's dynamic features. Using a centerless lathe as an example, this study establishes dynamic models for a cutterhead cutting system and a mechanical transmission system.

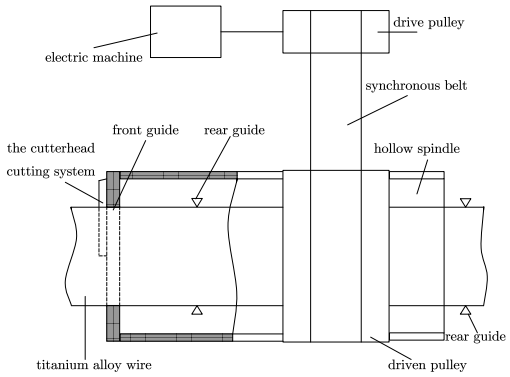

Fig. 1.Structure of the finishing process equipment

Dynamic modeling of the cutterhead cutting system

Fig. 2 shows a structural diagram of the cutterhead cutting system in the finishing process equipment. The system consists of the cutterhead providing support, the cutting tool holder (clamping box) for the cutting tool embedded in the cutterhead's dovetail groove, and the press block that secures the cutting tool holder in place. Each of the four cutting tool holders is equipped with cutting tools, which are bolted to the cutting tool holder. During the assembly process, the tangential position of the cutting tool holder is fixed by the press block, and the radial position is fixed by the cutterhead cutting system.

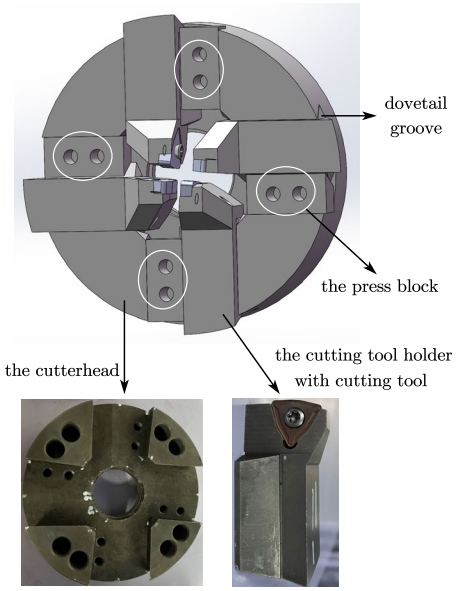

Fig. 2. Structural diagram of the cutterhead cutting system in the finishing process equipment

The following assumptions are made based on the structure of the centerless lathe cutterhead cutting system, as illustrated in Fig. 3: (1) The cutterhead cutting system is composed of four subsystems, which are primarily based on cutting tool holders 1, 2, 3, and 4. (2) Cutting tool holders 1, 2, 3, and 4 share identical fundamental characteristics. (3) Assume rigid contact between the press block and the cutterhead, as well as between the cutting tool holder and the cutterhead, without regard for stiffness damping. (4) Mass-spring-damping systems replace the contacts between the tool tip and the bar, the cutting tool holder and the cutterhead cutting system's periphery, and the cutting tool holder and the press block. Figure 3 shows the dynamic model of the cutterhead cutting system that was established.

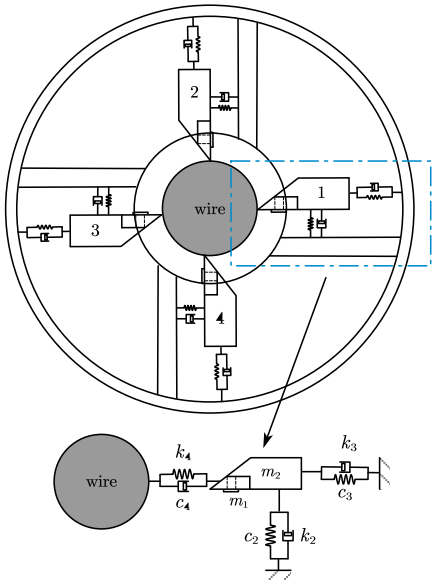

Fig. 3. Dynamic modeling of the cutterhead cutting system

Where m_1 and m_2 represent the equivalent masses of cutting tool 1 and cutting tool holder 1, respectively, c_2 and k_2 represent the damping and stiffness in the tangential direction of the cutting tool holder, c_3 and k_3 represent the damping and stiffness in the radial direction of the cutting tool holder, c_4 and k_4 represent the damping and stiffness in the radial direction of cutting tool.

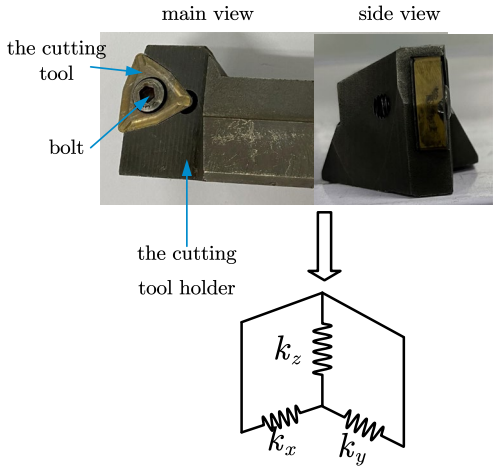

Fig. 4. Equivalent modeling of the bolted connection interface

The cutting tool holder experiences cutting vibrations in the groove as a result of the workpiece's reaction forces during turning process. Given the radial and tangential vibration displacements, the cutterhead cutting system is simplified to a two-degree-of-freedom system in the x and y dimensions, as illustrated in Fig. 5 and Fig. 6.

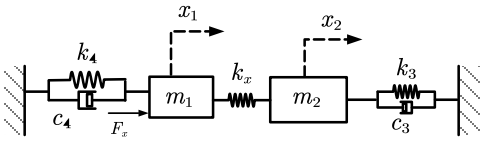

Fig. 5. Dynamic model of the cutting tool and its cutting tool holder in the x-direction

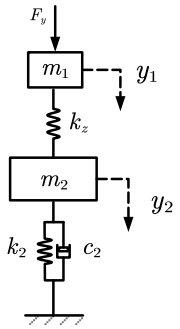

Fig. 6. Dynamic model of the cutting tool and its cutting tool holder in the y-direction

Where k_x and k_z represent the stiffness of the bolted connection interface in the x and z directions, F_x is the cutting force of the cutterhead cutting system in the radial direction of the cutting tool holder, and F_y is the cutting force of the cutterhead cutting system in the tangential direction of the cutting tool holder.

Using cutting tool 1's static equilibrium position as the coordinate origin, the force equilibrium relationship yields the differential equation for the two-degree-of- freedom cutting vibration in the x-direction:

$$\begin{cases} m_1\ddot{x}_1 + c_4\dot{x}_1 + k_4x_1 + k_{1x}\left(x_1 - x_2\right) = F_x \\ m_2\ddot{x}_2 + c_3\dot{x}_2 + k_3x_2 - k_{1x}\left(x_1 - x_2\right) = 0 \end{cases} \tag{1}$$

To avoid the coupled vibration effects of m_1 and m_2 in the y-direction from impacting the overall system's dynamic response, their displacement errors must be within 0.1 mm. The differential equations for the 2-degree-of-freedom cutting vibration are given below. Using numerical simulation to solve these equations, the y-directional vibration displacements of m_1 and m_2 are determined to be 0.0537 mm and 0.0533 mm, respectively, which are within the acceptable error range. As a result, an unfixed-end model, as shown in Fig. 6, can be used to more properly assess and regulate the system's vibration behavior.

$$\begin{cases} m_1\ddot{y}_1 + k_{1z}\left(y_1 - y_2\right) = F_y \\ m_2\ddot{y}_2 + c_2\dot{y}_2 + k_2y_2 - k_{1z}\left(y_1 - y_2\right) = 0 \end{cases} \tag{2}$$

Modeling of the mechanical transmission system

In the finishing process equipment, the synchronous belt transmission system relies on the contact between the belt wheel and the belt with high precision to transfer power smoothly and drive the load rotation, but the viscoelastic and polygon effect of the synchronous belt during the rotating movement will cause the longitudinal transmission error in the transmission process, so the theoretical analysis mainly studies the longitudinal vibration of the transmission system. Ignore the transverse elastic deformation of the drive shaft. The pulley only considers the moment of inertia, and ignores the damping and friction in the system, and the driving wheel and the driving wheel rotate around their own fixed rotating axes.

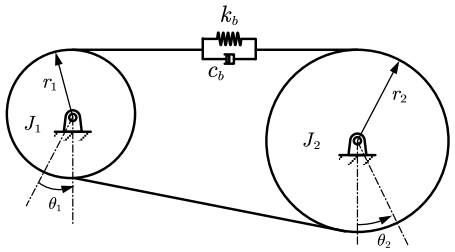

Fig. 7. Torsional vibration model for a synchronous toothed belt drive

Where k_b and c_b represents the stiffness and damping coefficient of the synchronization belt, θ_1 and θ_2, r_1 and r_2 are the angular displacement and radius of the main and driven wheels respectively, J_1 and J_2 are the moment of inertia of the main and driven wheels around their fixed rotating axes respectively.

Differential equation of rotation motion of driving wheel and driven wheel:

$$\begin{aligned} J_1\ddot{\theta}_1 + c_b\left(\dot{\theta}_1 - \dot{\theta}_2\right) + k_b\left(\theta_1 - \theta_2\right) &= T_1 \\ J_2\ddot{\theta}_2 - c_b\left(\dot{\theta}_1 - \dot{\theta}_2\right) - k_b\left(\theta_1 - \theta_2\right) &= -T_2 \end{aligned} \tag{3}$$

Where T_1 and T_2 bear the torque of the main and slave wheels respectively.

GETTING PARAMETERS FOR THE MECHANICAL DYNAMICS MODELS

Determining the damping and stiffness of the tool and its holder

This study employs modal hammer testing to assess the damping and stiffness of the tool and its

holder. The following engineering requirements dictated the selection of the German equipment: the m+p SO Analyzer—a data acquisition and modal analysis platform; the 5800B4 model modal hammer; and the Dytran 3097A2 accelerometer sensor. The data gathering and analysis platform, modal hammer, and accelerometer sensor are connected to the mechanical structure modal analysis system instrument, resulting in the entire modal testing platform illustrated in Fig. 8.

Fig. 8.Modal hammer testing platform

After completing the parameter identification procedure in the SmartOffice modal analysis software package system, the analysis findings are saved to obtain damping and natural frequencies in the x and y directions of the tool and tool holder, as shown in Table 1.

Table 1.Modal hammer test results

	Frequency/Hz	**Damping**
Cutting tool x-direction	735.34	1.20%
Cutting tool holder x-direction	1387.23	4.71%
Cutting tool holder y-direction	1337.03	2.22%

Based on the natural frequency, the equivalent stiffness of the cutting tool in the x-direction is calculated as:

$$k_4 = 4\pi^2 m f^2 = 170776 N/m \tag{4}$$

Similarly, the corresponding stiffness of the cutting tool holder in the x and y-directions is:

$$\begin{aligned} k_3 &= 4\pi^2 m f^2 = 35783069 N/m \\ k_2 &= 4\pi^2 m f^2 = 33240148 N/m \end{aligned} \tag{5}$$

Determining the stiffness at the bolted connection interface

In the study of stiffness at the bolted connection interface, scholars have summarized specific formulas and empirical data for calculating joint stiffness under certain conditions (Cai et al, 2014). Masataka Yoshimura showed that when the average contact pressure at the bonding interface is the same, their unit area dynamic characteristics are similar, and their equivalent stiffness and damping can be obtained by integrating parameters of the bonding interface.

As shown in Fig. 9, under bolt preloading, the contact pressure distribution function at the connection interface can be expressed by the following equation (Gaul et al, 2001):

$$\begin{aligned} p(r) &= aFe^{\left(-\frac{(r-b)^2}{c^2}\right)} \\ F &= \frac{T}{kd} \end{aligned} \tag{6}$$

Where T is the bolt torque, k is the torque coefficient, usually taken as 0.2, d is the nominal diameter of the bolt, a, b, and c are fitting parameters that are independent of the preload force F value (Marshall et al, 2006).

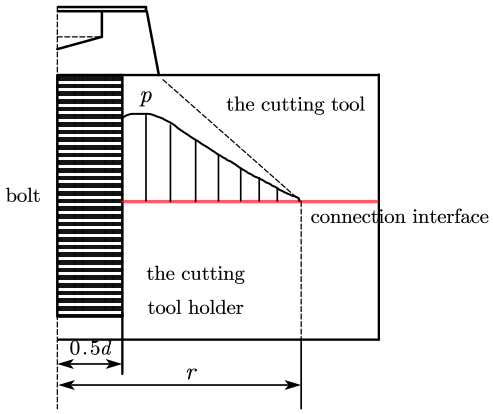

Fig. 9. Distribution of the contact pressure at the connection interface

Research indicates (Wang et al, 2013) that the connection interface stiffness is closely related to the contact pressure, and the following relationship exists:

$$k_1(p) = \alpha p^{\beta}(r) \tag{7}$$

Based on the above equation, according to Masataka Yoshimura's method, the following formula for calculating the tangential stiffness of the connection interface is obtained:

$$\begin{cases} K_x = K_y = \int_{r_h}^{r_m} 2\pi r \alpha_2 \left(aFe^{\left(\frac{(r-b)^2}{c^2}\right)} \right)^{\beta_2} dr \\ K_z = \int_{r_h}^{r_m} 2\pi r \alpha_1 \left(aFe^{\left(\frac{(r-b)^2}{c^2}\right)} \right)^{\beta_1} dr \end{cases} \tag{8}$$

Where r_h and r_m are the minimum and maximum radii of the contact pressure distribution at the connection interface, respectively, r is the radius of the contact pressure distribution, α_1 and β_1 , α_2 and β_2 are constants related to the properties of the connection interface.

According to reference (Marshall et al, 2006), take $a = 0.8$, $b = 4.8$, $c = 16$, $r_h = 4mm$, and $r_m = 7.2mm$. $\alpha_1 = 20644$, $\beta_1 = 1.7$, $\alpha_2 = 561280$, $\beta_2 = 0.31$. The bolt torque $T = 20N \cdot m$ and substituting the above parameters into the equation yields the tangential stiffness of the bolted connection interface as:

$$\begin{cases} K_x = K_y = 6.67 \times 10^6 N/m \\ K_z = 1.40 \times 10^6 N/m \end{cases} \tag{9}$$

Fitting of the empirical formulas for the cutting forces

Because the centerless lathe is turning titanium alloy wire, the cutting process is extremely complicated and there are many influencing factors. Therefore, at present, a unified calculation formula has not been formed, and the cutting force is calculated according to the empirical formula.

The calculation formula for the main cutting force and the cutting resistance are as follows:

$$F_s = 2931.355 \alpha_p \cdot f^{0.54} \cdot \sin^{0.46} k_\tau \tag{10}$$

$$F_p = 2/5 F_s \tag{11}$$

Where α_p is the cutting depth, f is the feed rate, and k_τ is the main deflection angle of the tool, where $k_\tau = 30^\circ$.

In the x-direction, the excitation force on the system arises from the difference in forces between two opposing cutting tools, which is caused by varying cutting depths (Δa) and thus differing cutting resistances. This difference is denoted as ΔF_p . Therefore, the force in the x-direction is:

$$F_x \cdot \Delta a = F_p \cdot \Delta a \tag{12}$$

In the y-direction, the excitation force on the system arises from the difference in forces between two opposing cutting tools, which is caused by varying cutting depths (Δa) and thus differing main cutting forces. This difference is denoted as ΔF_s. Therefore, the force in the y-direction is:

$$F_y \cdot \Delta a = F_s \cdot \Delta a \tag{13}$$

ELECTROMECHANICAL COUPLING DYNAMICS MODELING

Establishment of the motor model

To establish a dynamic model of a permanent magnet synchronous motor in the dq coordinate system, the Park transformation is used to transform the three-phase voltage of the motor stator into a two-phase rotating dq coordinate system. The electrical parameters of the permanent magnet synchronous motor are also discounted to the dq-axis equivalent circuit model, and the corresponding voltage equations, flux linkage equations, and electromagnetic torque equations are as follows.

The voltage equation:

$$\begin{cases} u_d = \frac{d}{dt}\psi_d - \omega_r \psi_q + R_s i_d \\ u_q = \frac{d}{dt}\psi_q - \omega_r \psi_d + R_s i_q \end{cases} \tag{14}$$

The flux linkage equation is:

$$\begin{cases} \psi_d = L_d i_d + \psi_f \\ \psi_q = L_q i_q \end{cases} \tag{15}$$

The electromagnetic torque equation is:

$$T_e = \frac{3}{2} p \left[\psi_f i_q - \left(L_d - L_q \right) i_d i_q \right] \tag{16}$$

Where i_d, i_q, u_d, u_q, ψ_d, ψ_q are the components of stator current, voltage and stator flux of permanent magnet synchronous motor in dq two-phase rotating coordinate system, respectively, w_r is the rotor angular velocity, L_d 、 L_q are stator winding d and q axis inductors. For hidden pole synchronous motor, $L_d = L_q$, so the electromagnetic torque can be expressed as：

$$T_e = \frac{3}{2} p \psi_f i_q \tag{17}$$

Electromechanical coupling model

By partially simplifying the electric system of the motor and the transmission system of the synchronous belt, a 4-degree-of-freedom model of the synchronous belt driving-motor rotor vibration considering the tensile stiffness of the synchronous belt and the torsional stiffness of the drive shaft is established. The motor rotor shaft is connected with the

synchronous belt driving wheel, and the driven wheel is connected with the load (hollow spindle and cutterhead cutting system connected with it), so that the motor rotation can drive the load rotation, as shown in Fig. 10. In the figure, J_e 、 J_1 、 J_2 and J_L are respectively the moment of inertia of the motor, the driving wheel, the driven wheel and the load. θ_1、 θ_2、 θ_e and θ_L are respectively the rotation angles of the main driving wheel, the driving wheel, the motor and the load. k_{d1}、 k_{d2} and k_b are the torsional stiffness of the input shaft, the output shaft and the tensile stiffness of the synchronization belt, respectively. c_{d1}、 c_{d2} and c_b are the torsional damping parameters of input axis, output axis and synchronous belt damping parameters respectively. T_e 、 T_1 、 T_2 and T_L are respectively motor torque, driving wheel torque, driven wheel torque and load torque. With θ_1、 θ_2、 θ_e and θ_L as generalized coordinates, the system dynamics equations are obtained from Newton's second law.

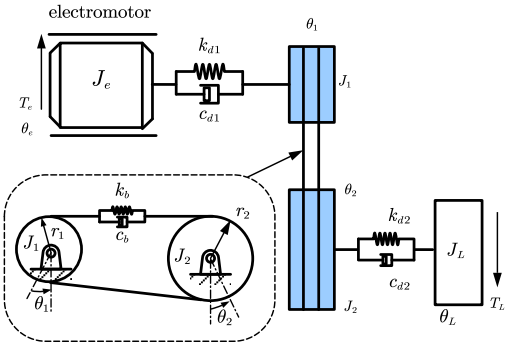

Fig. 10. Dynamic modeling of the motor-cutterhead cutting system

$$\begin{cases} J_e\ddot{\theta}_e + c_{d1}\left(\dot{\theta}_e - \dot{\theta}_1\right) + k_{d1}\left(\theta_e - \theta_1\right) = T_e \\ J_1\ddot{\theta}_1 - c_{d1}\left(\dot{\theta}_e - \dot{\theta}_1\right) - k_{d1}\left(\theta_e - \theta_1\right) = -T_1 \\ J_2\ddot{\theta}_2 + c_{d2}\left(\dot{\theta}_2 - \dot{\theta}_L\right) + k_{d2}\left(\theta_2 - \theta_L\right) = T_2 \\ J_L\ddot{\theta}_L - c_{d2}\left(\dot{\theta}_2 - \dot{\theta}_L\right) - k_{d2}\left(\theta_2 - \theta_L\right) = -T_L \end{cases} \tag{18}$$

Taking electromagnetic torque and cutting system torque as driving torque and load torque respectively and acting on the synchronous belt transmission system through the motor shaft and the drive shaft, the resulting driven wheel torque fluctuation acts on the cutting system through the output shaft. Combining equations (1), (2), (3), (14)-(18), the electromechanical coupling dynamics model of the dynamic cutting system of the finishing machining equipment is established. The specific expression is as follows:

$$\begin{cases} u_d = \dfrac{d}{dt}\psi_d - \omega_r\psi_q + R_s i_d \\ u_q = \dfrac{d}{dt}\psi_q - \omega_r\psi_d + R_s i_q \\ \psi_d = L_d i_d + \psi_f \\ \psi_q = L_q i_q \\ T_e = \dfrac{3}{2}p\left[\psi_f i_q - \left(L_d - L_q\right) i_d i_q\right] \\ M\ddot{X} + \left(C_i + C_b\right)\dot{X} + \left(K_i + K_b\right)X = T \end{cases} \tag{19}$$

Where X is the generalized degree of freedom the system, M is the generalized mass matrix of the system, K_i and K_d are equivalent stiffness matrix and torsional stiffness matrix respectively, C_i and C_d are equivalent damping matrix and torsional damping matrix respectively, T is the external torque matrix composed of T_e and T_L.

Selection of model parameters

Some of the parameters of the system are shown in Table 2.

Table 2.Partial system parameters

Parameters	Value
Motor moment of inertia $J_e / (kg \cdot m^2)$	1.9×10^{-2}
Load moment of inertia $J_L / (kg \cdot m^2)$	6.7×10^{-2}
Synchronous belt pulley moment of inertia J_1、$J_2 / (kg \cdot m^2)$	2.7×10^{-3}
	2.7×10^{-2}
Modules of belt pulley m / mm	2
Number of teeth of belt pulley Z_1、Z_2	20, 30
Torsional damping ratio	0.05
Torsional stiffness k_{d1}、$k_{d2} / (N \cdot m / rad)$	1×10^5
	1×10^5
Tensile stiffness $k_b / (N \cdot m / rad)$	2.75×10^7

SIMULATION MODELS

Building the dynamics simulation model

The MATLAB/Simulink modules are used to solve the differential equations listed in previous chapters, and a simulation model is constructed, as shown in Fig. 11.

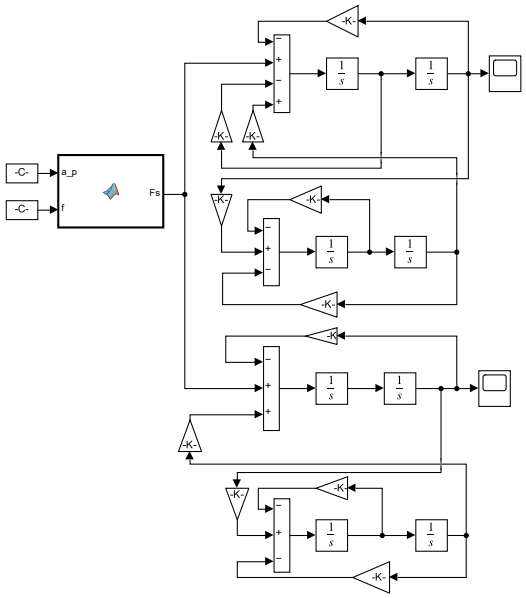

Fig. 11.Dynamic simulation model

Table 3.The main parameters of the permanent magnet synchronous motor

Parameters	Value
Rated power P/kw	3
Rated speed w/rpm	1200
Number of pole pairs n_p	4
Stator resistance $/\Omega$	0.958
Damping coefficient $B/N\cdot M\cdot s$	0.008
Bus voltage U_{dc}/V	311
d-axis inductance L_d/mH	5.25
q-axis inductance L_d/mH	12
Permanent magnet flux linkage φ_f/wb	0.1827

Building the electromechanical coupling simulation model

MATLAB/Simulink was used to solve the electromechanical coupling model: first, the Simulink module was used to build a permanent magnet synchronous motor and its current-hysteresis-control model; second, the S-function was used to establish the dynamics equations of the motor-synchronous belt transmission system, with external excitation such as electromagnetic torque as the input to the system; and third, the electromagnetic torque produced by the permanent magnet synchronous motor acted on the dynamic system, from which the motor rotor angular velocity was computed. This angular velocity is then fed back into the motor system, thus completing the establishment of the electromechanically coupled model. The Simulink simulation model is constructed as shown in Fig. 12, with the main motor parameters detailed in Table 3.

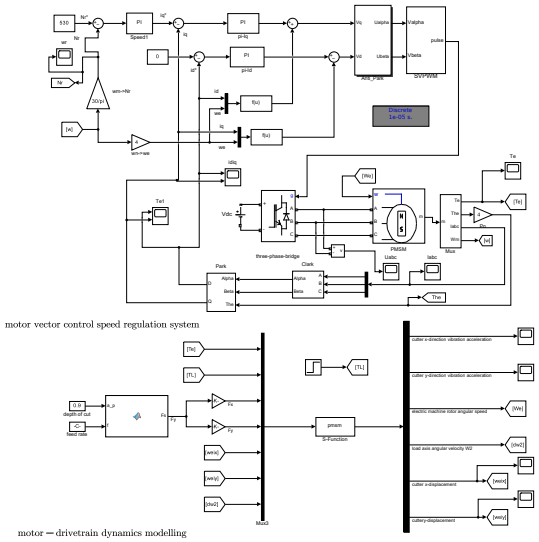

Fig. 12. Simulation model of the motor-synchronous belt transmission system

Verification of simulation models

To verify the correctness of the above modeling method, an electro-mechanical coupling simulation experimental platform for finishing process equipment is first built, as shown in Fig. 13. The vibration signal acquisition system consists of three main components: the accelerometer mounted on the machine tool, the matched high-precision data acquisition instrument, and the DASP system software. The data collected by the accelerometer is transmitted to a computer, where it is processed using the DASP software to complete the vibration signal acquisition.

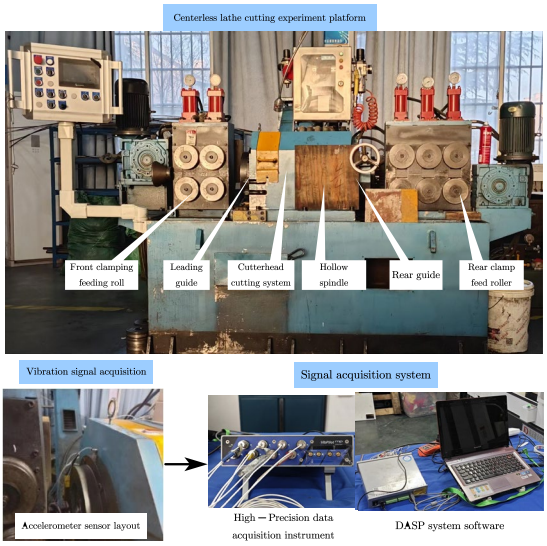

Fig. 13.Build an experimental platform

According to the practical engineering requirements, a TB9 wire with a diameter of approximately 8mm, a length of 90m, and having undergone rough machining is selected as the test material. The cutting tool chosen is a YG8 carbide turning tool. During the cutting process, the motor speed is set to 530 r/min, the feed rate to 0.5 m/min, and the cutting depth to 0.9 mm. The vibration signal at the front end of the spindle bearing seat (i.e., the x-direction of the cutterhead cutting system) is collected under these operating conditions. The same conditions are applied in the mechanical dynamic simulation and electromechanical coupling simulation, and appropriate step-size algorithms are used to solve both simulation systems. In the process of collecting vibration signal, it will be interfered by the external environment, experimental equipment and various factors, so the signal must be pre-processed such as removing trend, processing transient and denoising. The model parameters of the dynamic cutting system of the centerless lathe in this study are the same as those in reference (Shi et al, 2023), and under the same working conditions, the time-domain amplitude and characteristic frequency distribution of the vibration acceleration response at the tool are consistent with the test results.

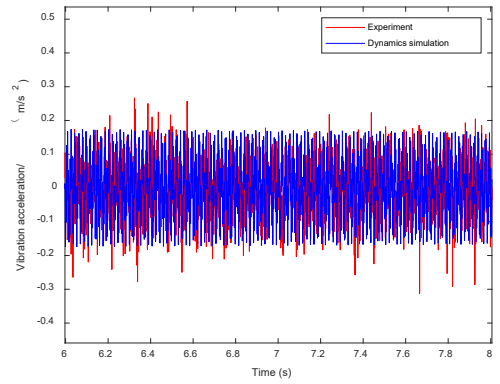

(a)

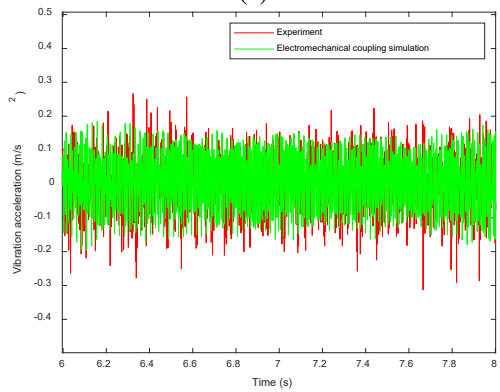

(b)

Fig. 14. Time domain diagram of cutting tool x-direction vibration acceleration under different models

Fig. 14 (a) shows the comparison between the experimental results and the mechanical dynamics simulation results. During the experiment, the vibration acceleration of the cutting tool fluctuates in the range of -0.3~0.3m/s^2, and the simulation results fluctuate in the range of -0.17~0.17m/s^2. Combined with the signal frequency components in Fig. 15 (a), it can be seen that the main frequency of mechanical dynamics simulation is the gear meshing frequency f_m and its double frequency, while the vibration signal of the experiment also includes the current frequency of the motor f_e. When the mechanical dynamics model of cutting system is established, the effect of electrical system is not taken into account, so its performance in time-frequency domain is different from the experiment results.

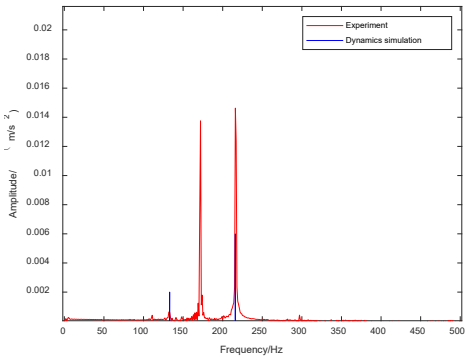

(a)

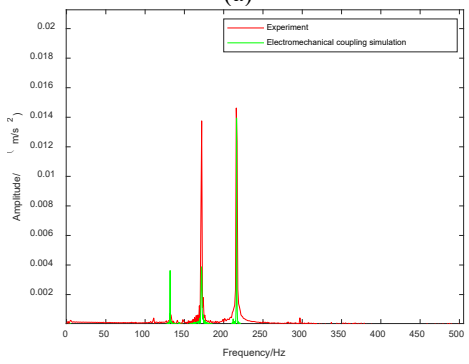

(b)

Fig. 15. Frequency domain diagram of cutting tool x-direction vibration acceleration under different models

Fig. 14 (b) and Fig. 15 (b) respectively show the time-frequency and frequency comparison diagrams of the vibration acceleration at the cutting tool. During the electromechanical coupling simulation, the vibration acceleration at the cutting tool fluctuates within the range of -0.2~0.2m/s^2. The main frequency components are the gear mesh frequency f_m and its double frequency, and the current frequency of the motor f_e. Through the above comparison, it can be

found that the system characteristics shown in the experiment are consistent with the dynamic characteristics of the electromechanical coupling simulation.

The cutting tool vibration signals obtained by experiment and electromechanical coupling simulation are non-stationary signals, and more attention should be paid to their frequency components, which may change with time. Therefore, it is necessary to compare experimental and electromechanical coupling simulation vibration signals in the time-frequency domain to better capture the local features and frequency changes within the signals. Therefore, wavelet packet analysis is chosen in this study. Fig. 16 (a) and (b) show that the experimental vibration signals are mainly concentrated in the low-frequency range, although the high-frequency band is also involved. In contrast, the electromechanical coupling simulation signals are concentrated below 300 Hz in the low-frequency range. This difference arises because experimental signals are affected by factors such as noise and instability. However, these differences are within a reasonable range, indicating that the electromechanical coupling simulation signal behaves similarly to the experimental signal in the time-frequency domain.

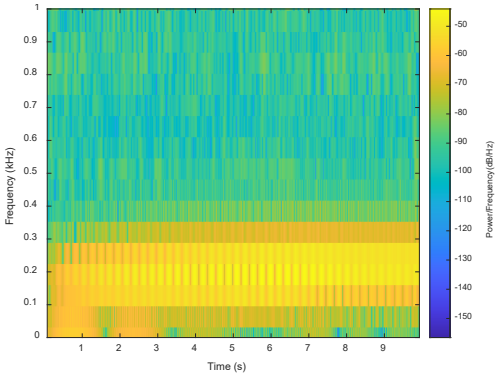

(a) Experiment

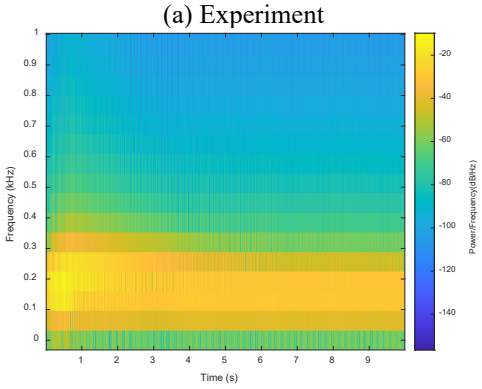

(b) Electromechanical coupling simulation

Fig. 16. Time-frequency diagram of cutting tool x-vibration acceleration

Through the above comparisons, it can be observed that the electromechanical coupling simulation model exhibits system characteristics that are essentially consistent with the experimental vibration signals. This confirms the accuracy of the electromechanical coupling model established in this study.

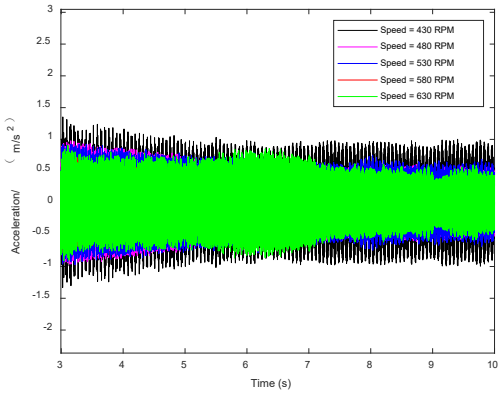

(a)

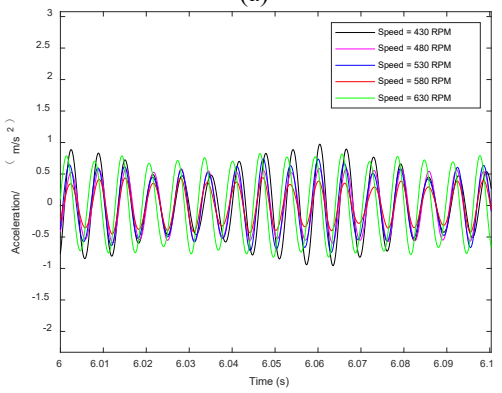

(b)

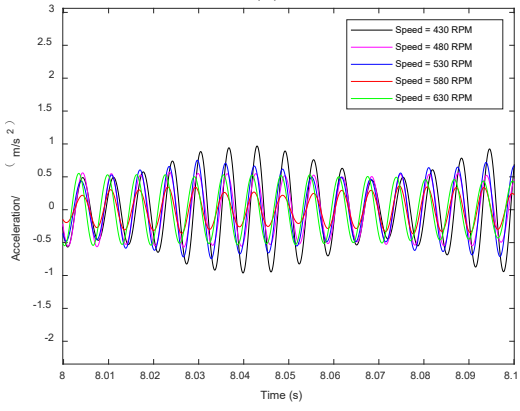

(c)

Fig. 17. Fluctuations in acceleration vibration signals at different motor speeds

ANALYSIS OF SYSTEM DYNAMIC CHARACTERISTICS

In summary, the electromechanical coupling model better reflects the actual vibration characteristics of the system, so the following research is conducted based on the system's electromechanical coupling model. In this model, the vibration characteristics of

the system can be observed by changing mechanical and electrical parameters. However, although electrical parameters can be adjusted, their impact on the system's vibration characteristics is more complex and less intuitive compared to mechanical parameters. Therefore, this paper mainly analyzes the effects of mechanical parameters (motor speed, feed rate, and cutting depth) on the x-direction vibration acceleration and displacement of the cutterhead cutting system.

Vibration Characteristics of the System at Different motor speeds

In the electromechanical coupling simulation, the cutting depth is fixed at 0.9mm, and the feed rate is set to 0.5m/min. The motor speeds are set to 430r/min, 480r/min, 530r/min, 580r/min, and 630r/min, respectively, and the vibration in the cutting tool x-direction is observed. By varying the motor speed, the vibration magnitude and trend of the cutting system are studied, which helps to adjust the system parameters to improve machining accuracy.

When analyzing the electromechanical coupling simulation vibration signals, large impacts and transient effects may occur during the first 3 seconds due to system startup or other factors. To obtain more accurate vibration characteristics of the system, this study only considers the data between 3 and 10 seconds. Fig. 17 shows the acceleration vibration signal fluctuations at different motor speeds. It can be observed that by changing the motor speed, the cutting tool's vibration acceleration in the x-direction undergoes significant changes. From Fig. 17(a), it can be seen that at a motor speed of 580r/min, the acceleration fluctuation range is the smallest, ranging from -0.4 to 0.4m/s². This suggests that at this speed, the motor control, feedback control, and other system parameters are likely optimized, resulting in the most stable system operation.

Fig. 18 shows the curve of the average acceleration values as a function of the motor speed. This analysis considers the changes in average acceleration due to the variations in two variables: motor speed and cutting depth. It is evident from the graph that with increasing motor speed, the trends in the average acceleration values are generally consistent across different cutting depths. For motor speeds ranging between 430rpm and 530rpm, the average acceleration increases with speed for various cutting depths. At 530rpm, the average acceleration reaches its maximum because at this motor speed, the system approaches its resonance frequency (f_r), $f_r = f_n\sqrt{1-2\xi^2} = 61.5\times\sqrt{1-2\times0.57^2} \approx 35.2Hz$, leading to significant vibration. When the motor speed increases from 530rpm, the system gradually moves away from the resonance frequency, weakening the resonance effect. Consequently, the average vibration acceleration decreases, reaching its minimum at 580r/min, where the system operates most stably, consistent with the results shown in Fig. 17.

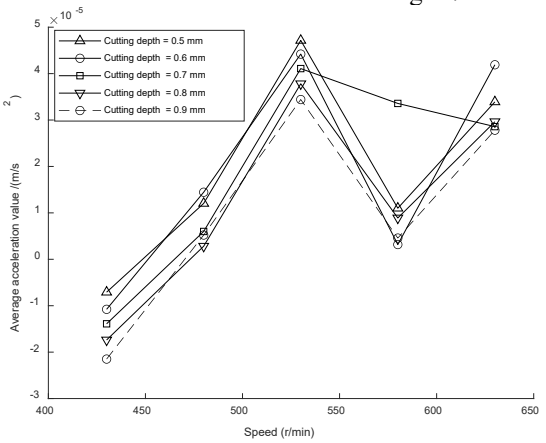

Fig. 18. Curves of the average acceleration as a function of the motor speed

Through electromechanical coupling simulation and mechanical dynamics simulation, the cutting tool vibration signal in x-direction (i.e., radial direction of cutterhead cutting system) is obtained. By changing the motor speed (530r/min, 580r/min, 630r/min) to study the vibration size and vibration trend of the cutting system, and then improve the surface quality of the centerless lathe workpiece. In order to verify the accuracy of the simulation results of the mechanical dynamics model and the electromechanical coupling model, they are compared with the experimental results, as shown in Table 4.

Table 4. Comparison of x-direction experimental parameters and simulation parameters

Motor speed (r/min) / Mean displace-ment(mm)	530	580	630
Mechanical dynamics simulation	4.18×10^{-2}	3.73×10^{-2}	3.50×10^{-2}
Experiment	3.97×10^{-2}	3.47×10^{-2}	3.64×10^{-2}
Error rate	5.29%	7.49%	3.85%
Electromecha-nical coupling simulation	3.90×10^{-2}	3.56×10^{-2}	3.72×10^{-2}
Error rate	1.76%	2.59%	2.20%

$$\delta = \frac{S_a - E}{E} \tag{20}$$

Where δ refers to the error rate, S_a refers to the mean

of theoretical displacement, E refers to the mean of experimental displacement.

The vibration data of cutting system in x-direction is obtained by experiments, and compared with the simulation data of mechanical dynamics and electromechanical coupling. It can be seen from the Table 4 that when the speed is changed, the error rate between the experimental value and the theoretical value of the vibration of the mechanical dynamics model reaches a maximum of 7.5% because the influence of the motor is not considered. The error rate of electromechanical coupling model is less than 5% because the electrical parameters and control parameters are taken into account. Among them, when the motor speed is 580r/min, the simulation data and the experimental data can draw the conclusion that the vibration displacement at the cutting tool is minimum under this condition. According to the Table 4, the cutting stability in the x-direction is better at motor speeds of 580r/min and 630r/min. However, as the motor speed increases, tool wear also increases. Therefore, the optimal cutting stability is achieved at a motor speed of 580r/min. In conclusion, considering the cutting tool wear, the motor speed can be appropriately increased to ensure machining accuracy while balancing the cutting tool longevity.

Vibration Characteristics of the System at Different feed rates

The vibration characteristics of the centerless lathe cutterhead cutting system exhibit significant changes in the x-direction at different feed rates (with other parameters kept constant, a fixed depth of cut of 0.9mm, and motor speed set to 580rpm). The feed rates are set to 0.5m/min, 0.6m/min, 0.7m/min, 0.8m/min, and 0.9m/min, and the vibration magnitude and trends are observed with changes in feed rate. Based on this, adjustments to the cutting system parameters are made to improve machining accuracy.

Fig. 19 shows the fluctuation of the system's vibration acceleration at different feed rates. From Fig. 19(a), it can be seen that within the first 8 seconds, the acceleration fluctuation range for feed rates between 0.5m/min and 0.8m/min is roughly the same, while the acceleration fluctuation range at 0.9m/min is significantly smaller than at the other feed rates. From Fig. 19(c), it is observed that at 9 seconds, the acceleration fluctuation at 0.9m/min gradually approaches the fluctuations seen at other feed rates. This phenomenon suggests that, in the initial stage, the vibration acceleration fluctuation is smaller at higher feed rates. However, as time progresses and cutting conditions change, the acceleration fluctuation at higher feed rates gradually increases.

Fig. 20 shows the curve of the average acceleration value changing with feed rate, considering the impact of both motor speed and feed rate on the average acceleration. It can be observed that as the feed rate increases, the trend of the average acceleration value remains relatively consistent across different motor speeds, indicating that the feed rate has a minimal impact on the average acceleration value. At a motor speed of 580 rpm, the average acceleration value performs the best, with the smallest average acceleration values occurring at feed rates of 0.5m/min and 0.6m/min. This suggests that under these cutting conditions, the cutting process is relatively stable.

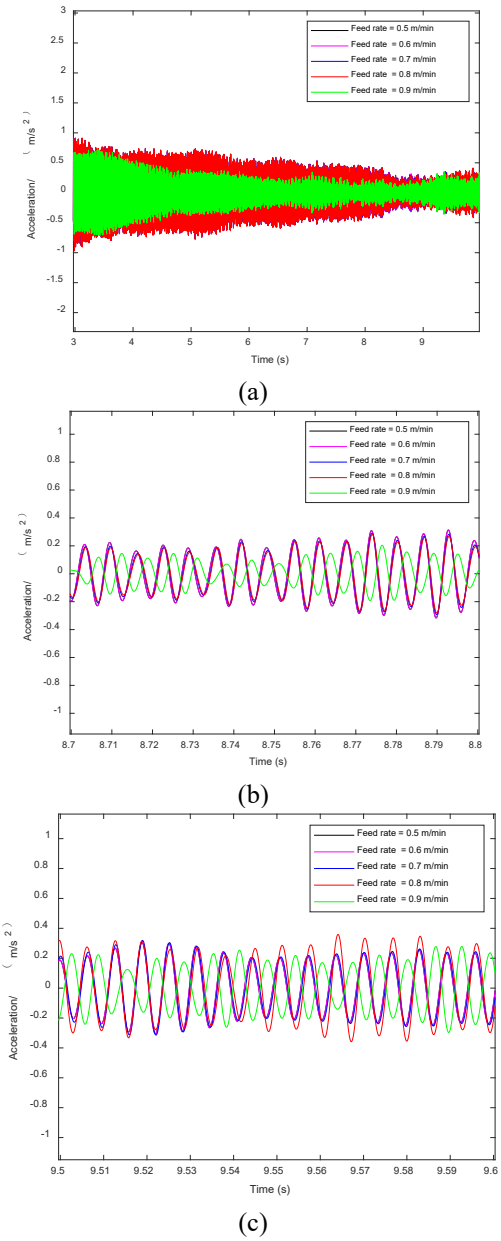

(a)

(b)

(c)

Fig. 19. Fluctuations of acceleration vibration signals at different feed rates

Through electromechanical coupling simulation and mechanical dynamics simulation, the cutting tool vibration signal in x-direction (i.e., radial direction of cutterhead cutting system) is obtained. The various of vibration displacement of cutting system was observed by changing the feed rate (0.5m/min, 0.7m/min, 0.9m/min). Table 5 compares the change of the mean

value of vibration displacement of cutterhead cutting system with the change of feed speed under different models.

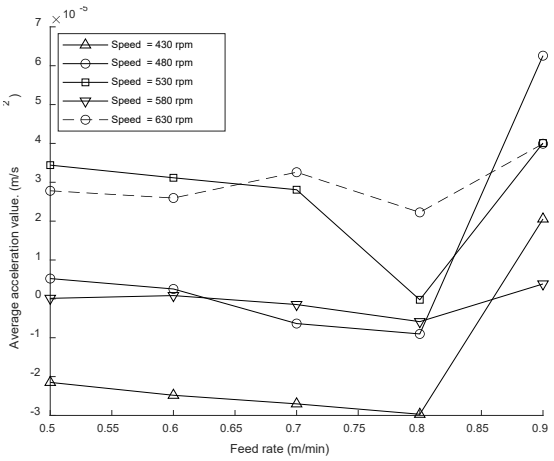

Fig. 20. Curves of the average acceleration as a function of the feed rate

Table 5 Comparison of x-direction experimental parameters and simulation parameters

Feed rate (m/min) / Mean Displace-ment(mm)	0.5	0.7	0.9
Mechanical dynamics simulation	3.76×10^{-2}	4.13×10^{-2}	3.99×10^{-2}
Experiment	3.63×10^{-2}	3.97×10^{-2}	3.83×10^{-2}
Error rate	3.58%	4.03%	4.18%
Electromecha-nical coupling simulation	3.69×10^{-2}	4.02×10^{-2}	3.91×10^{-2}
Error rate	1.65%	1.26%	2.09%

As can be seen from the Table 5, when the feed rate is 0.5m/min, the average vibration displacement obtained by mechanical dynamics simulation is 3.76×10^{-2}, and the average value obtained by electromechanical coupling simulation is 3.69×10^{-2}, while the experimental average value is 3.63×10^{-2}. The error rate of mechanical dynamics simulation is 3.58%, and the error rate of electromechanical coupling simulation is 1.65%. When the feed rate is 0.7m/min, the average vibration displacement obtained by mechanical dynamics simulation is 4.13×10^{-2}, and the average value obtained by electromechanical coupling simulation is 4.02×10^{-2}, while the experimental average value is 3.97×10^{-2}. The error rate of mechanical dynamics simulation is 4.03%, and the error rate of electromechanical coupling simulation is 1.26%. With the feed rate increased to 0.9m/min, the average vibration displacement obtained by mechanical dynamics simulation is 3.99×10^{-2}, and the average value obtained by electromechanical coupling simulation is 3.91×10^{-2}, while the experimental average value is 3.83×10^{-2}. It can be found that the error rate of mechanical dynamics simulation reaches 4.18%, and the error rate of electromechanical coupling simulation also increases to 2.09%.

Through calculation, the error between the simulation value and the experimental value in x-direction of the cutterhead cutting system is less than 5%, but the mean displacement error under electromechanical coupling simulation is smaller and closer to the experimental value. This shows that changing the feed speed will not have much effect on the vibration response of the system. According to the above analysis, the change trend of vibration displacement of the system is the smallest when the feed speed is 0.5m/min, so the feed speed can be appropriately reduced to improve the machining accuracy.

CONCLUSIONS

This paper presents an electromechanical coupling dynamic model which can be applied to the cutting system of finishing process equipment under variable speed and variable load conditions. The effect of changing cutting parameters on the dynamic characteristics of the motor-load coupling system is analyzed. The main conclusions are as follows:

(1)When the motor speed ranges from 430r/min to 630r/min, the system acceleration fluctuation range can be observed. It can be found that the acceleration fluctuation range is the minimum under 580r/min. When the motor speed increases from 430r/min to 530r/min, the mean of acceleration increases with the motor speed, and the minimum vibration acceleration occurs at 580r/min. Under this condition, the error rate between the average vibration displacement under the mechanical dynamics simulation model and the experimental value is 7.49%, and the error rate between the average vibration displacement under the electromechanical coupling simulation model and the experimental value is 2.59%. The error rate of the mean displacement and the experimental value under the electromechanical coupling simulation is less than 3%, which verifies the accuracy of the electromechanical coupling model.

(2)The fluctuation range of acceleration under different feed rates is basically consistent with the change trend of the mean acceleration, and the change of vibration displacement is also very small, which indicates that the feed rate has little influence on the dynamic characteristics of the system. The

error rate between the mean displacement and the experimental value under the mechanical dynamics simulation is less than 5%, and the error between the mean displacement and the experimental value under the electromechanical coupling simulation is less than 2.09%, and the result of the electromechanical coupling simulation is closer to the experimental value.

(3)When the motor speed is 580 r/min and the feed speed is 0.5m/min, the acceleration fluctuation range and the mean of displacement are the smallest. In summary, taking into account the processing efficiency, the motor speed can be appropriately increased and the feed speed reduced to ensure the processing accuracy.

ACKNOWLEDGMENT

The authors thank the supported by the Key Research and Development Project of Shaanxi Province, China (2023-YBGY-386).

REFERENCES

Altintas, Y., Stepan, G., Merdol, D., and Dombovari, Z., "Chatter Stability of Milling in Frequency and Discrete Time Domain," CIRP Journal of Manufacturing Science and Technology 1.1: 35–44 (2008).

Cai, L.G., Hao, Y., Guo, T.N., Liu, Z.F., and Zhang, D.M., "Method of Extracting Normal Static Stiffness of Bolted Joint Interfaces." Journal of Vibration and Shock 33.16: 18–23 (2014).

Chen, R.B., Liu, C.Z., and Qing, D.D, "Mechanical-rigid-flexible coupling dynamic characteristics of integrated gear-generator system for wind power." Acta Energiae Solaris Sinica 44.7: 328–338 (2023).

Feki, N., Clerc, G., and Velex, Ph., "An Integrated Electro-Mechanical Model of Motor-Gear Units—Applications to Tooth Fault Detection by Electric Measurements." Mechanical Systems and Signal Processing 29: 377–390 (2012).

Feki, N., Clerc, G., and Velex, Ph., "Gear and Motor Fault Modeling and Detection Based on Motor Current Analysis." Electric Power Systems Research 95: 28–37 (2013).

Fu, J.N., Li, G.F., and Ye, C.H., "Simulation and Analysis of Tooth Engagement Pressure of Synchronous Belt." Journal of Mechanical Strength 45.3: 743–749 (2023).

Gao, W.J., "Impact of Cold Drawing Deformation and Aging on Microstructure and Mechanical Property of TB9 Titanium Alloy." World Nonferrous Metals 12: 154–155 (2020).

Gaul, L., and Nitsche, R., "The Role of Friction in Mechanical Joints." Applied Mechanics Reviews 54.2: 93–106 (2001).

Heege, A., "Computation of Dynamic Loads in Wind Turbine Power Trains." DEWI-Magazin (2003).

Kanaan, H.Y., Al-Haddad, K., and Roy, G., "Analysis of the Electromechanical Vibrations in Induction Motor Drives Due to the Imperfections of the Mechanical Transmission System." Mathematics and Computers in Simulation, Modelling and Simulation of Electric Machines, Converters and Systems 63.3: 421–433 (2003).

Li, M., Feng, W.Z., Guan, L., Wang, X., Zhang, Y.Q., and Wang, J., "Summary of Titanium Alloy for Fastener in Aerospace." Nonferrous Metal Materials and Engineering 39.4: 49–53 (2018).

Liu, C.Z., Qin, D.D., Lim, T.C., and Liao, Y.H., "Dynamic Characteristics of the Herringbone Planetary Gear Set during the Variable Speed Process." Journal of Sound and Vibration 333.24: 6498–6515 (2014).

Marshall, M.B., Lewis, R., and Dwyer-Joyce, R.S., "Characterisation of Contact Pressure Distribution in Bolted Joints." Strain 42.1: 31–43 (2006).

Mishra, A., Yau, H.-T., Kuo, P.-H., and Wang, C.-C., "Achieving Sustainability by Identifying the Influences of Cutting Parameters on the Carbon Emissions of a Milling Process." The International Journal of Advanced Manufacturing Technology 135.11: 5409–5427 (2024).

Ozlu, E., and Budak, E., "Analytical Modeling of Chatter Stability in Turning and Boring Operations—Part I: Model Development." Journal of Manufacturing Science and Engineering 129.4: 726–732 (2007a).

Ozlu, E., and Budak, E., "Analytical Modeling of Chatter Stability in Turning and Boring Operations—Part II: Experimental Verification." Journal of Manufacturing Science and Engineering 129.4: 733–739 (2007b).

Peng, T.-J., Kuo, P.-H., Huang, W.-C., and Wang, C.-C., "Nonlinear Dynamic Analysis and Forecasting of Symmetric Aerostatic Cavities Bearing Systems." International Journal of Bifurcation and Chaos, World Scientific Publishing Company (2024).

Qing, S.A., Zhou, P., Zhou, Y.J., and Jiang, H.Y., "Summary of the Development of Belt Drives Industry." Journal of Mechanical Transmission 44.8: 1–7 (2020).

Ren, D.C., Liu, Y.J., Zhang, H.B., Wang, J., Jin, W., and Yang, R., "Influence of Cold Deformation and Aging Heat Treatment on Microstructure and Mechanical Property of TB9 Titanium Alloy." Rare Metal Materials and Engineering 49.3: 1083–1089 (2020).

Shi, L.C., Li, J.X., Liu, Y.X., Jia, R.X., and Dou, W.T., "Experimental study on the relationship between vibration characteristics and surface roughness of TB9 titanium alloy milling system." Surface Technology 51.6: 354–363 (2022).

Shi, L.C., Zhang, Q., Liu, T.F., Liu, Y.X., and Lu, Z.Q., "Study on Stability of Surface Turning Finishing Processes of Titanium Alloy Wires Based on Process Damping." China Mechanical Engineering 34.16: 1936–1945 (2023).

Wang, C.-C., Kuo, P.-H., Peng, T.-J., Oshima, M., Cuypers, S., and Chen, Y.-T., "Voting Model Prediction of Nonlinear Behavior for Double-Circumferential-Slot Air Bearing System." Chaos, Solitons & Fractals 183: 114908 (2024).

Wang, J.R., and Zhang, D.Q., "Modeling and Dynamic Characteristics Analysis of Synchronous Belt Transmission Mechanism in PVC Clamping and Stepping Device for Packaging Machine." Machinery Design & Manufacture 10: 203–208 (2024).

Wang, L., Du, R., Jin, T., Liu, H.T., Niu, J., and Zhao, W.H., "Study on matching design of bolted joint fixing surfaces." Journal of Xi'an Jiaotong University 47.7: 62–67 (2013).

Wang, X.Y., Zhang, L., Xu, H.W., Song, S.W., and Zhang, Y.T., "Effect of Bolt Pre-tightening Force on Dynamic Characteristics of Vibration Test Fixture." Journal of Rocket Propulsion 46.6: 69–75 (2020).

Zhu, H., Zhu, W.D., and Fan, W., "Dynamic Modeling, Simulation and Experiment of Power Transmission Belt Drives: A Systematic Review." Journal of Sound and Vibration 491: 115759 (2021).